


Cite this: *RSC Adv.*, 2020, 10, 41410

Design of a new multi-functional catalytic system Ni/SO₃H@zeolite-Y for three-component synthesis of *N*-benzo-imidazo- or -thiazole-1,3-thiazolidinones†

Mehdi Kalhor * and Soodabeh Banibairami

In this investigation, a nanoporous zeolite-NaY supported sulfonic acid was synthesized and Ni(II) ions were successfully stabilized on SO₃H@zeolite-Y (Ni/SO₃H@zeolite-Y). This novel type of zeolitic nanocomposite was characterized using various techniques including FT-IR, FE-SEM, TGA, BET and EDX. Ni/SO₃H@zeolite-Y was used as a multi-functional and highly active nanocatalyst for the three-component synthesis of 3-benzimidazolyl-1,3-thiazolidin-4-ones and new 3-benzthiazolyl-1,3-thiazolidin-4-ones via cyclocondensation of 2-aminobenzimidazole or 2-aminobenzothiazole, aromatic aldehydes and thioglycolic acid in acetone-H₂O at room temperature. This economical chemical procedure has advantages such as excellent yield in short reaction times, convenient manipulation and high purity of products, applicability to a broad range of substrates, and the use of a nontoxic and heterogeneous acid catalyst with good reusability.

Received 26th September 2020

Accepted 6th November 2020

DOI: 10.1039/d0ra08237f

rsc.li/rsc-advances

1. Introduction

In recent years, crystalline porous materials have attracted increasing interest due to their applications in petrochemicals, environmental technologies and chemical reactions, particularly for catalytic strategies. These porous compounds include zeolites, ordered mesoporous silica, and metal-organic frameworks. The main features of these materials are high adsorption capacity, active sites with different strengths, uniform channels and cavities, and electronic properties.¹ Among them, the zeolites have recently considered as heterogeneous catalysts or ideal supports for homogeneous catalysts due to their high surface area, high thermal-stability, nanoporous crystalline structure, persistence in all organic solvents, no waste or disposal problems, less or no corrosion, easy set-up of continuous processes and *etc.*^{2,3}

From 1962 to now, zeolite-NaY has received considerable concerns in fluid catalytic cracking (FCC) and gasoline production due to its high surface area, strong acidity, high hydrothermal stability, and low cost.¹ Recently, zeolite-NaY has used as ideal supports for homogeneous catalysts such as alkylaminopyridine-grafted on HY zeolite and application in synthesis of 4*H*-chromenes,⁴ Ni@zeolite-Y for the synthesis of 1,3-thiazolidinones,⁵ nano-CuY zeolite for facile synthesis of

perimidines,⁶ metal loaded Y-zeolite for thermo-catalytic pyrolysis of real end of life vehicle plastics waste,⁷ micro-mesoporous zeolite catalysts for alkylation,⁸ Cu@zeolite/magnetic for the synthesis of 1,2,3-triazoles,⁹ Pd@zeolite-Y for Suzuki-Miyaura coupling of aryl halides with phenylboronic acid.¹⁰

Given the importance of zeolite as a suitable mineral support, SO₃H-modified mesoporous zeolites have been successfully applied in many catalytic reactions,¹¹ direct methanol fuel cell application¹² and as temperature tolerant proton conducting materials.¹³ Furthermore, Ni-based mesoporous zeolites have been reported for catalytic synthesis for example biomass pyrolysis,¹⁴ CO₂ methanation,¹⁵ selective ring opening of 1-methylnaphthalene,¹⁶ hydrodeoxygenation and hydrocracking of microalgae biodiesel¹⁷ and *etc.*⁵ Recently, zeolite-Y has been used as the supported surface of bi-functional nanocatalyst.¹⁸ This is very important in synthetic chemistry, that way, the multiple types of active sites can be created on a single nanocatalyst.¹⁹ To the best of our knowledge, there is no example for the synthesis of activated zeolite-NaY by the combination of Ni species and SO₃H groups in its structure and its catalytic application in the synthesis of heterocycles.

Thiazolidinone heterocycles are saturated form of thiazole that have a sulfur atom at position 1, a nitrogen atom at position 3 and a carbonyl group at position 2, 4, or 5. The thiazolidinone scaffolds are responsible for many various biologically active heterocyclic compounds. A carbonyl group in position four, creates 4-thiazolidinone derivatives which are used widely in synthetic chemistry and pharmaceutical compounds. They exhibit number of activities such as antitubercular, anti-

Department of Organic Chemistry, Payame Noor University, Tehran, 19395-4697, Iran.
E-mail: mekalhor@gmail.com; Fax: +98 2537179170; Tel: +98 2537179170

† Electronic supplementary information (ESI) available. See DOI: 10.1039/d0ra08237f



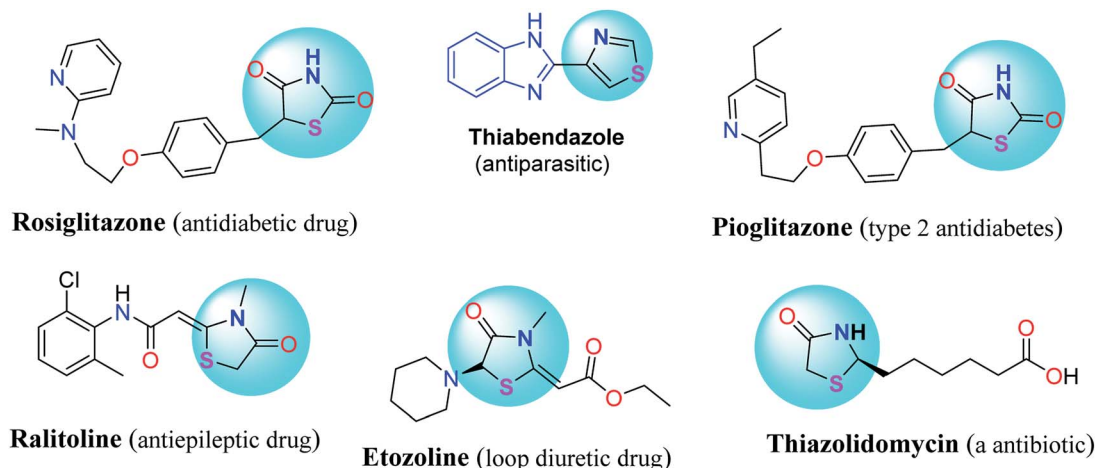


Fig. 1 Some example of drugs containing of 1,3-thiazolidin-4-one.



Scheme 1 Synthetic method for 1,3-thiazolidin-4-ones using Ni/SO₃H@zeolite-Y.

convulsant, antimicrobial, anti-inflammatory, anticancer, antiviral agents, and as anti-HIV agents.^{20–24} Fig. 1 shows some drug structures based on thiazolidinone. This versatile applicability highlights the importance of access to efficient synthetic routes to well benign the substituted thiazolidin-4-one compounds. The classical synthesis reported can be either a one-pot or a two-step process through condensation of amines and aromatic aldehydes, and thioglycolic acid. Although various heterogeneous and homogeneous catalysts have been applied for the substituted 1,3-thiazolidin-4-ones,^{24–38} synthesis of new thiazolidine heterocycles and exploration for greener and cleaner synthetic strategies still remains as an active research.

Having these facts and since today the design of new multifunctional nanocatalysts is one of the hot area of research, herein, we decided to report synthesis of Ni/SO₃H@zeolite-Y through loading nickel ions on SO₃H-functionalized zeolite-NaY (SO₃H@zeolite-Y) as a novel and very promising solid acid (Lewis and Brønsted acid) nanocatalyst in the efficient preparation of *N*-benzimidazolyl-1,3-thiazolidin-4-ones (**4a–j**). Also, this catalytic method was used for the synthesis of 3-benzothiazolyl-1,3-thiazolidin-4-ones (**4k–p**), as new thiazole based heterocyclic scaffolds (Scheme 1).

2. Experimental

2.1. Chemicals and apparatus

All chemicals were purchased from the Merck and Fluka Chemical Companies. The products were identified by

comparing the physical data with those of known samples or by their spectral data. IR spectra were obtained with KBr disc on a JASCO FT-IR 4200-A spectrophotometer. ¹H NMR and ¹³C NMR spectra were recorded on Bruker spectrophotometer (300 or 500 MHz) in DMSO-*d*₆ using Me₄Si as internal standard. Field emission-scanning electron microscopic (FE-SEM) images were performed on a Zeiss Sigma FE-SEM that it equipped with energy dispersive X-ray spectrometer (EDX). Nitrogen adsorption and desorption isotherms (BET analysis) were measured at 196 °C by a USA Micromeritics (MicroActive for TriStar II Plus Version 2.03, Serial # 283) system after the samples were vacuum dried at 150 °C overnight. The TGA/DTA measurements were carried out by using a Bahr (Wetzlar, Germany) STA-503 instrument. TGA/DTA runs were recorded at a scan rate of 10° min^{−1} up to 1000 °C under pure argon atmosphere.

2.2. Synthesis of Ni/SO₃H@zeolite-Y

SO₃H@zeolite-Y was prepared as follows: a 500 mL suction flask was charged with 1.5 g of zeolite-NaY and equipped with a constant pressure dropping funnel containing 2 mL of chlorosulfonic acid. The chlorosulfonic acid was added dropwise manner to zeolite-NaY over a period of 30 min at 0 °C under N₂ atmosphere. After the addition was complete, the mixture was shaken for 45 min. Then, the mixture was washed with dichloromethane and H₂O under ultrasound irradiation and dried at 50 °C to obtain nano SO₃H@zeolite-Y. The loaded Ni on SO₃H@zeolite-Y was prepared by ion-

exchange process. Typically, 1.0 g $\text{SO}_3\text{H@zeolite-Y}$ in a 150 mL flask was added to an aqueous solution of $\text{NiCl}_2 \cdot 2\text{H}_2\text{O}$ (2 mM, 50 mL) at ambient temperature. The mixture was stirred for 20 h and then it was filtered. The resulting precipitate was washed repeatedly with water until negative reaction of Cl^- using AgNO_3 test. The $\text{Ni}/\text{SO}_3\text{H@zeolite-Y}$ nanocomposite was placed under ultrasound irradiations for 30 min, and then dried at 70°C for 2 h.

2.3. General procedure for the preparation of 1,3-thiazolidin-4-ones

A mixture of aldehyde (1 mmol), 2-aminobenzimidazole or 2-aminobenzothiazole (1.1 mmol), thioglicolic acid (1.2 mmol) and 5%w the $\text{Ni}/\text{SO}_3\text{H@zeolite-Y}$ (0.007 g) in 5 mL H_2O /acetone (1 : 1) was mixed at room temperature. After satisfactory completion of the organic reaction (TLC monitoring using hexane and ethyl acetate (2 : 1) as eluents), The catalyst was separated by simple filtration and filtrate was added to 10 mL of cold water and precipitate was filtered off and washed with cold ethanol-water mixture. The desired product was purified by recrystallization in ethanol-water and air dried. The known 1,3-thiazolidin-4-one products were characterized by comparing the results of physical and spectroscopic data with those of the authentic samples. The new *N*-benzothiazole-1,3-thiazolidinones were identified by FT-IR, ^1H NMR, ^{13}C NMR and mass spectroscopy.

2.4. Spectroscopic data for the new compounds

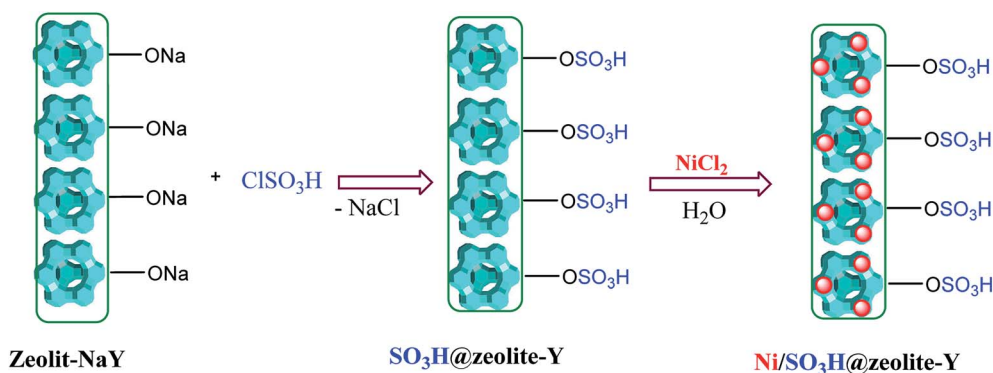
2.4.1. 3-(1*H*-Benzo[d]imidazol-2-yl)-2-(2-nitrophenyl)thiazolidin-4-one (4c). FT-IR (KBr) (ν_{max}): 3437, 3338 (NH), 2929 (C-H), 1703 (C=O), 1650, 1540 (C=N), 1520, 1338 (NO_2), 1455, 1369 (C=C), 1118 (C-N), 1024, 668 (C-S-C) cm^{-1} ; ^1H -NMR (500 MHz, $\text{DMSO}-d_6$) δ_{H} : 3.39 (1H, d, $J = 16.55$ Hz, SCH_2), 4.21 (1H, d, $J = 16.55$ Hz, SCH_2), 7.06 (3H, d br, CH and H-Ar), 7.43 (2H, s br, H-Ar), 7.47 (1H, d, $J = 7.90$ Hz, H-Ar), 7.55 (1H, t, $J = 7.55$ Hz, H-Ar), 8.17 (1H, d, $J = 8.10$ Hz, H-Ar), 12.51 (1H, br, NH) ppm; ^{13}C -NMR (125 MHz, $\text{DMSO}-d_6$) δ_{C} : 32.2, 58.2, 122.2, 126.0, 126.1, 129.8 (2C), 135.5, 137.2 (2C), 144.8, 146.8, 172.1 ppm; MS (m/z , %): 340 (M^+ , 30), 294 (32), 220 (65), 206 (30), 178 (25), 160 (100), 133 (25), 104 (18), 90 (20), 77 (18).

2.4.2. 3-(1*H*-Benzo[d]imidazol-2-yl)-2-(2-chlorophenyl)thiazolidin-4-one (4g). IR (KBr) (ν_{max}): 3444, 3349 (NH), 2925 (C-H), 1683 (C=O), 1535 (C=N), 1447, 1303, 1269 (C=C), 1170 (C-N), 743, 647 (C-S-C) cm^{-1} ; ^1H -NMR (500 MHz, $\text{DMSO}-d_6$) δ_{H} : 3.97 (1H, d, $J = 16.50$ Hz, SCH_2), 4.11 (1H, d, $J = 16.45$ Hz, SCH_2), 6.85 (1H, s, CH), 7.06–7.15 (3H, m, H-Ar), 7.24 (1H, t, $J = 7.55$ Hz, H-Ar), 7.30 (1H, t, $J = 7.60$ Hz, H-Ar), 7.38 (1H, d, $J = 7.90$ Hz, H-Ar), 7.53 (2H, t, $J = 7.60$ Hz, H-Ar), 12.52 (1H, s, NH) ppm; ^{13}C -NMR (125 MHz, $\text{DMSO}-d_6$) δ_{C} : 32.1, 59.5, 112.4, 118.2, 122.0, 122.2, 125.2, 128.1, 129.9, 130.5, 131.5, 133.3, 138.3, 140.2, 144.7, 172.2 ppm; MS (m/z , %): 329 (M^+ , 10), 294 (100), 252 (30), 220 (94), 135 (30), 118 (20), 91 (18).

2.4.3. 3-(Benzo[d]thiazol-2-yl)-2-(2-hydroxyphenyl)thiazolidin-4-one (4k). IR (KBr) (ν_{max}): 1700 (C=O), 1532 (C=N), 1381, 1269 (C=C), 1117 (C-N), 655 (C-S-C) cm^{-1} ; ^1H -NMR (300 MHz, $\text{DMSO}-d_6$) δ_{H} : 3.95 (1H, d, $J = 16.59$ Hz, SCH_2), 4.09 (1H, d, $J = 16.56$ Hz, SCH_2), 6.68 (1H, t, $J = 7.28$ Hz, CH), 6.83 (3H, q, $J = 8.78$ Hz, H-Ar), 7.08 (1H, t, $J = 7.42$ Hz, H-Ar), 7.28–7.40 (2H, m, H-Ar), 7.64 (1H, d, $J = 7.8$ Hz, H-Ar), 7.99 (1H, d, $J = 7.58$ Hz, H-Ar), 10.12 (1H, s, OH) ppm; ^{13}C -NMR (75 MHz, $\text{DMSO}-d_6$) δ_{C} : 32.3, 59.5, 115.6, 118.8, 121.2, 121.8, 124.2, 125.0, 126.2, 126.4, 128.9, 131.3, 147.7, 154.2, 156.0, 172.1 ppm; MS (m/z , %): 328.6 (M^+ , 48), 255.6 (100), 237.6 (9.3), 177.5 (21), 137.5 (27), 108.4 (11), 91.5 (8).

2.4.4. 3-(Benzo[d]thiazol-2-yl)-2-(3-nitrophenyl)thiazolidin-4-one (4l). IR (KBr) (ν_{max}): 1690 (C=O), 1617, 1537 (C=N), 1467, 1369, 1274 (C=C), 1349, 1530 (NO_2), 1228 (C-N), 658 (C-S-C) cm^{-1} ; ^1H -NMR (300 MHz, $\text{DMSO}-d_6$) δ_{H} : 4.02 (1H, d, $J = 16.73$ Hz, SCH_2), 4.32 (1H, d, $J = 16.71$ Hz, SCH_2), 7.06 (1H, s, CH), 7.29–7.40 (2H, m, H-Ar), 7.62 (2H, t, $J = 7.78$ Hz, H-Ar), 7.86 (1H, d, $J = 7.77$ Hz, H-Ar), 8.00 (1H, d, $J = 7.45$ Hz, H-Ar), 8.10 (1H, q, $J = 1.35$ Hz, H-Ar), 8.34 (1H, s, H-Ar) ppm; ^{13}C -NMR (75 MHz, $\text{DMSO}-d_6$) δ_{C} : 171.6, 155.9, 147.8, 147.5, 143.4, 131.8, 131.2, 130.3, 126.4, 124.4, 122.9, 121.9, 121.2, 120.8, 61.8, 31.8 ppm; MS (m/z , %): 357.6 (M^+ , 100), 315.6 (57), 284.6 (62.5), 255.6 (32.6), 237.6 (32.7), 181.5 (33.2), 135 (56).

2.4.5. 3-(Benzo[d]thiazol-2-yl)-2-(4-nitrophenyl)thiazolidin-4-one (4m). IR (KBr) (ν_{max}): 1690 (C=O), 1617, 1537 (C=N), 1467, 1369, 1274 (C=C), 1349, 1530 (NO_2), 1228 (C-N), 658 (C-S-C) cm^{-1} ; ^1H -NMR (300 MHz, $\text{DMSO}-d_6$) δ_{H} : 4.03 (1H, d, $J = 16.73$ Hz, SCH_2), 4.28 (1H, d, $J = 16.67$ Hz, SCH_2), 7.03 (1H, s, CH), 7.29–7.41 (2H, m, H-Ar), 7.61 (1H, d, $J = 7.53$ Hz, H-Ar),



Scheme 2 Systematic approach for the preparation of $\text{Ni}/\text{SO}_3\text{H@zeolite-Y}$.



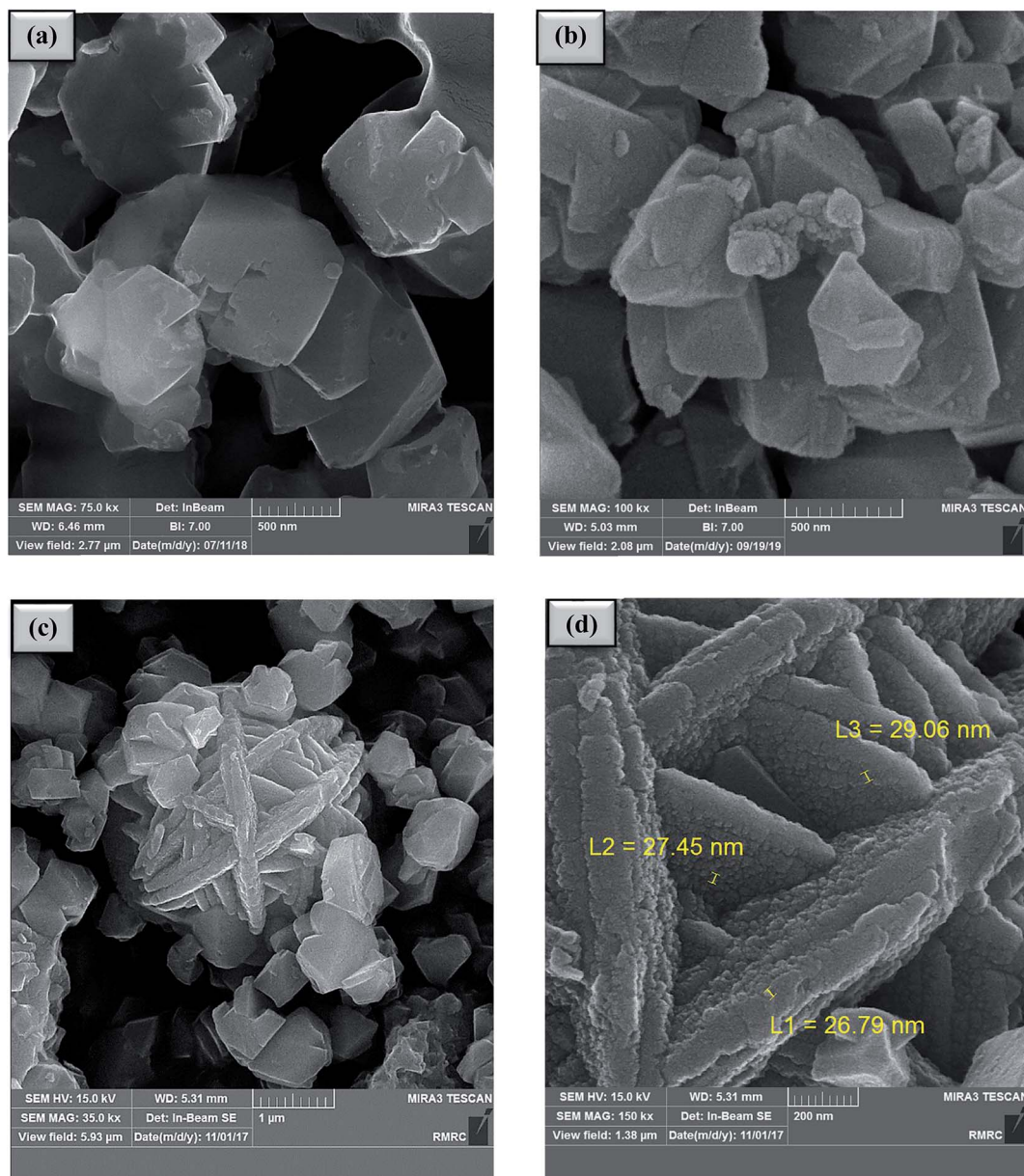


Fig. 2 FE-SEM images of (a) zeolite-NaY, (b) $\text{SO}_3\text{H}@$ zeolite-Y and (c), (d) $\text{Ni}/\text{SO}_3\text{H}@$ zeolite-Y. The EDX analysis of the $\text{Ni}/\text{SO}_3\text{H}@$ zeolite-Y is presented in Fig. 3. The quantitative results of elemental analysis confirm presence of the S, Ni, Al, Si, Na and O elements in zeolite structure. On the other hand, atomic absorption spectroscopy was performed to determine the concentration of Ni(II) ions loaded on $\text{SO}_3\text{H}@$ zeolite-Y which was 3.56 mmol g^{-1} (21%). Also, the number of acidic sites in the NZSA obtained 0.26 mmol g^{-1} using acid–base titration method.¹⁸

7.68 (2H, d, $J = 8.76 \text{ Hz}$, H-Ar), 8.01 (1H, q, $J = 1.18 \text{ Hz}$, H-Ar), 8.16 (2H, d, $J = 8.76 \text{ Hz}$, H-Ar) ppm; $^{13}\text{C-NMR}$ (75 MHz, $\text{DMSO-}d_6$) δ_{C} : 171.6, 156.0, 148.5, 147.5, 147.0, 131.2, 126.7, 126.4, 124.5, 124.0, 122.0, 121.2, 61.7, 31.9 ppm; MS (m/z , %): 357.1 (M^+ , 3.4), 108 (22.9), 69 (23.6), 46 (100).

2.4.6. 3-(Benzo[d]thiazol-2-yl)-2-(4-bromophenyl)thiazolidin-4-one (4n). IR (KBr) (ν_{max}): 1690 (C=O), 1617, 1537 (C=N), 1467, 1369, 1274 (C=C), 1228 (C-N), 658 (C-S-C) cm^{-1} ; $^1\text{H-NMR}$ (300 MHz, $\text{DMSO-}d_6$) δ_{H} : 3.99 (1H, d, $J = 16.76 \text{ Hz}$, SCH_2), 4.26 (1H, d, $J = 16.73 \text{ Hz}$, SCH_2), 6.89 (1H, s, CH), 7.30–7.41 (4H, m, H-Ar), 7.50 (2H, d, $J = 8.41 \text{ Hz}$, H-Ar), 7.63 (1H, d, $J = 8.75 \text{ Hz}$, H-Ar), 8.00 (1H, d, $J = 7.74 \text{ Hz}$, H-Ar) ppm; $^{13}\text{C-NMR}$ (75 MHz, $\text{DMSO-}d_6$) δ_{C} :

171.6, 155.9, 147.5, 140.6, 131.5, 131.2, 127.7, 126.3, 124.4, 121.9, 121.2, 121.0, 62.1, 31.8 ppm; MS (m/z , %): 392.4 (M^+ , 58.4), 350.4 (42.5), 317.4 (83.2), 181.5 (49.9), 161.5 (22.4), 135.5 (100), 108.4 (32.9).

2.4.7. 3-(Benzo[d]thiazol-2-yl)-2-(4-methoxyphenyl)thiazolidin-4-one (4o). IR (KBr) (ν_{max}): 1690 (C=O), 1617, 1537 (C=N), 1467, 1369, 1274 (C=C), 1228 (C-N), 658 (C-S-C) cm^{-1} ; $^1\text{H-NMR}$ (300 MHz, $\text{DMSO-}d_6$) δ_{H} : 3.69 (3H, s, OMe), 3.98 (1H, d, $J = 16.81 \text{ Hz}$, SCH_2), 4.26 (1H, d, $J = 16.79 \text{ Hz}$, SCH_2), 6.85 (1H, s, CH), 6.85 (2H, d, $J = 7.51 \text{ Hz}$, H-Ar), 7.29–7.42 (4H, m, H-Ar), 7.65 (1H, d, $J = 7.97 \text{ Hz}$, H-Ar), 7.99 (1H, d, $J = 7.69 \text{ Hz}$, H-Ar) ppm; $^{13}\text{C-NMR}$ (75 MHz, $\text{DMSO-}d_6$) δ_{C} : 171.6, 158.9, 155.9, 147.6, 132.9, 131.2, 127.0, 126.3,



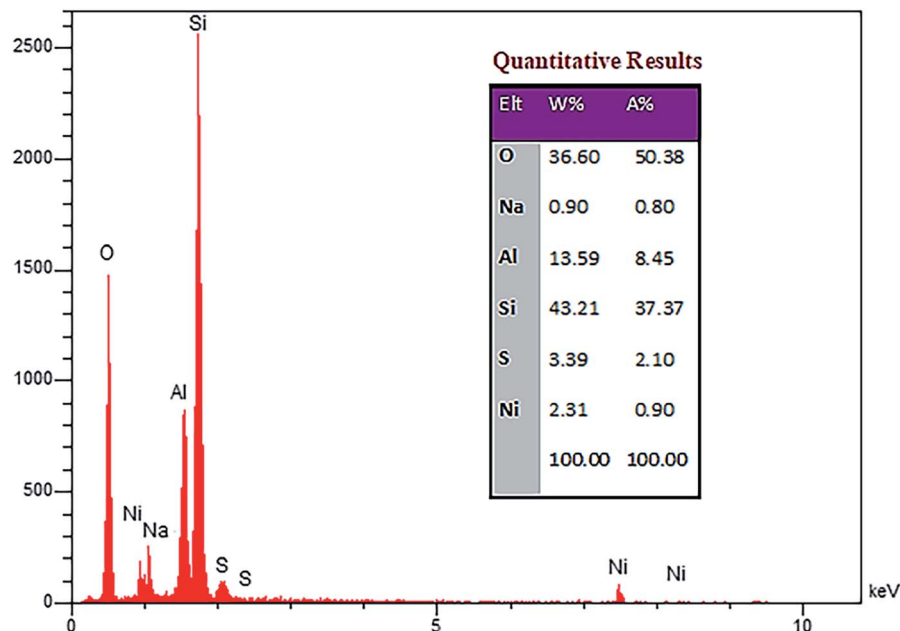


Fig. 3 EDX spectrum of the Ni/SO₃H@zeolite-Y.

124.3, 121.8, 121.2, 113.9, 62.5, 55.0, 31.9 ppm; MS (*m/z*, %): 342.6 (*M*⁺, 99.9), 300.6 (71.6), 267.6 (80.5), 208.5 (68.8), 181.5 (59.6), 151.5 (54.7), 135.5 (100), 108.4 (32.8).

2.4.8. 3-(Benzo[d]thiazol-2-yl)-2-(4-methylphenyl)thiazolidin-4-one (4p). IR (KBr) (ν_{max}): 1690 (C=O), 1617, 1537 (C=N), 1467, 1369, 1274 (C=C), 1228 (C-N), 658 (C-S-C) cm⁻¹; ¹H-NMR (300 MHz, DMSO-*d*₆) δ_{H} : 2.23 (3H, s, Me), 3.98 (1H, d, *J* = 16.78 Hz, SCH₂), 4.23 (1H, d, *J* = 16.75 Hz, SCH₂), 6.86 (1H, s, CH), 7.10 (2H, d, *J* = 7.99 Hz, H-Ar), 7.25–7.42 (4H, m, H-Ar), 7.64 (1H, d, *J* = 7.81 Hz, H-Ar), 7.99 (1H, q, *J* = 0.68 Hz, H-Ar) ppm; ¹³C-NMR (75 MHz, DMSO-*d*₆) δ_{C} : 171.7, 155.9, 147.6, 138.1, 137.3, 131.2, 129.2, 126.3, 125.3, 124.3, 121.9, 121.2, 62.6, 31.8, 20.6 ppm; MS (*m/z*, %): 326.5 (*M*⁺, 93.2), 284.5 (50.5), 251.5 (85), 181.5 (32.1), 135.5 (100), 91.5 (24.3), 69.4 (25.8).

3. Results and discussion

3.1. Synthesis and characterization of nanocatalyst

In this research, zeolite-NaY was functionalized with organic and inorganic species. As shown in Scheme 2, SO₃H@zeolite-Y was synthesized by the reaction of chlorosulfonic acid with zeolite-NaY under solvent-free conditions. Then, Ni(II) ions were stabilized on the SO₃H@zeolite-Y to produce a multi-functional nanohybrid with strong acidity. A systematic study was carried out for the characterization of the synthesized Ni/SO₃-H@zeolite-Y. Then the catalytic activity of SO₃H@zeolite-Y supported Ni was investigated for the synthesis of N-heterocyclic-1,3-thiazolidin-4-one. The number of acidic sites in the SO₃H@zeolite-Y obtained 0.26 mmol g⁻¹ using acid-base titration 18.

Fig. 2 shows the FE-SEM photographs of the zeolitic nanostructures. In Fig. 2a, it can be seen clearly that the zeolite-NaY has a crystalline structure. Fig. 2b shows that structure of

SO₃H@zeolite-Y nanocomposite is similar to that of the bare zeolite after functionalization with -SO₃H organic group. Also, Fig. 2c and d show after stabilization of Ni(II) ions, the crystalline and layer and layer structure with too pores for Ni/SO₃-H@zeolite-Y is still preserved. The average nanoparticles size is 26–29 nm, respectively.

The FT-IR spectra of zeolite-NaY, SO₃H@zeolite-Y and Ni/SO₃H@zeolite-Y are illustrated in Fig. 4. In the spectrum of zeolite-NaY, in Fig. 4a, the broad peak in 3459 cm⁻¹ region is related to the O–H stretching of hydrogen bonded internal silanol groups and hydroxyl stretching of water, while the peak at 1635 cm⁻¹ corresponds to the O–H group bending mode of water. Moreover, the peaks at 1021 and 792 cm⁻¹ are attributed to the symmetric and asymmetric stretching vibrations of the Si–O–Si groups, respectively.¹⁸ In the spectrum of SO₃-H@zeolite-Y in Fig. 4b, the broad peak at 3407 cm⁻¹ may be attributed to the –OH stretching vibration of the –SO₃H groups. While the peak at 1635 cm⁻¹ corresponds to bending mode of O–H of water. Beside those, the broad band at around 1080 cm⁻¹ corresponds to the Si–O stretching vibration and the asymmetric and symmetric stretching of S=O bond. The bands at 944 and 794 cm⁻¹ maybe assigned to the S–O bond. The displacement of IR bands to lower frequencies (red-shift) in the spectrum of Ni/SO₃H@zeolite-Y in Fig. 4c, as compared with SO₃H@zeolite-Y, confirm the exchange of a number of Ni²⁺ (heavier cation) with Na⁺ ion.⁵

The N₂ adsorption–desorption isotherm of zeolitic nanocomposites are shown in Fig. 5. The isotherms exhibit nitrogen types I isotherms which represents the microporous materials. Also, by looking at their hysteresis type, it can be seen that zeolitic structures have slits (layer and layer with high pores) structure and the initial nanostructure after the functionalize is still retained.^{18,39}



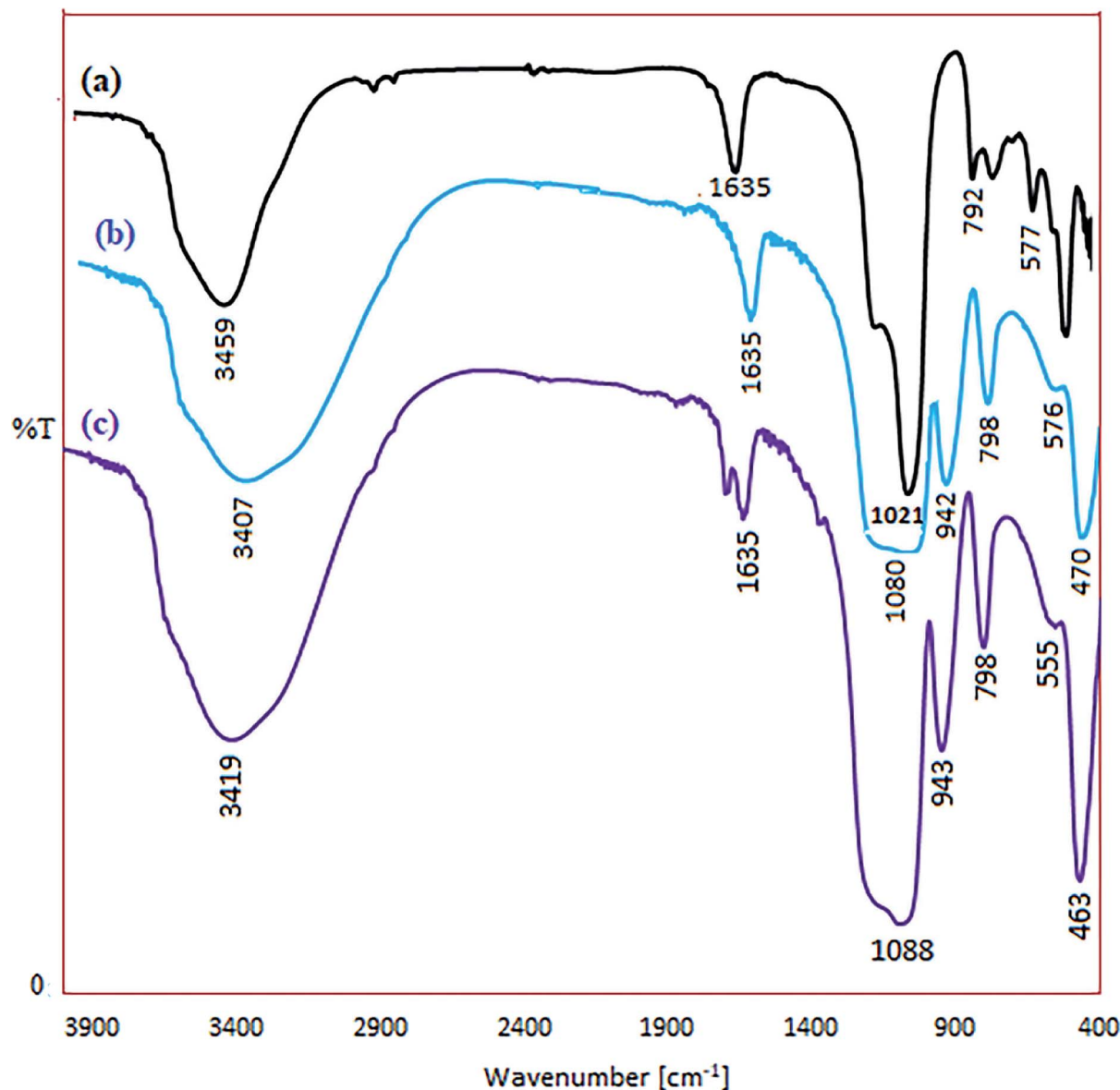


Fig. 4 The FT-IR spectra of (a) zeolite-NaY, (b) $\text{SO}_3\text{H}@zeolite\text{-}Y$ and (c) $\text{Ni}/\text{SO}_3\text{H}@zeolite\text{-}Y$.

The hybrid inorganic–organic nanostructure shows a pore size distribution in the range of 2–5.13 nm (Fig. 5c).

The textural properties of zeolitic frameworks are summarized in Table 1. Comparison of S_{BET} from $419 \text{ m}^2 \text{ g}^{-1}$ for zeolite-NaY to $285 \text{ m}^2 \text{ g}^{-1}$ for $\text{SO}_3\text{H}@zeolite\text{-}Y$ shows decrease in specific surface after modification with $-\text{SO}_3\text{H}$ and Ni functional groups.⁴⁰ The data at this table reveals that the S_{BET} of $\text{Ni}/\text{SO}_3\text{H}@zeolite\text{-}Y$ ($298 \text{ m}^2 \text{ g}^{-1}$) had increased slightly to its former modified structure. Furthermore, the $\text{SO}_3\text{H}@zeolite\text{-}Y$ has a lower pore volume in comparison with zeolite-NaY, which might be due to the presence of SO_3H groups on the pore surface. Also, this means that the SO_3H groups are grafted onto the pore wall surface of zeolite-NaY. This decrease of pore volume was also observed for the $\text{Ni}/\text{SO}_3\text{-H}@zeolite\text{-}Y$.

TGA curve of $\text{Ni}/\text{SO}_3\text{H}@zeolite\text{-}Y$ is presented in Fig. 6. The weight loss of 12.39% between the temperature intervals of 50–

185 °C is attributed to desorption of physical and chemical water molecules through endothermic process. The weight loss of 9.56% observed in the temperature range of 200–850 °C might be attributed to the removal of SO_3H groups in the zeolite framework.

3.2. Catalytic properties of catalyst

3.2.1. Optimization of reaction conditions. To determine the optimized reaction conditions, a one-pot reaction of 4-nitrobenzaldehyde, 2-aminobenzimidazole and thioglycolic acid was performed as the model reaction at room temperature in the presence of $\text{Ni}/\text{SO}_3\text{H}@zeolite\text{-}Y$. The results are listed in Table 2 which indicate the $\text{Ni}/\text{SO}_3\text{H}@zeolite\text{-}Y$ as a powerful nanocatalyst acted at ambient temperature so that 5wt% of the nanocatalyst in acetone/ H_2O (1 : 1) was optimum conditions (Table 2, entry 6). Comparing the zeolite-NaY,

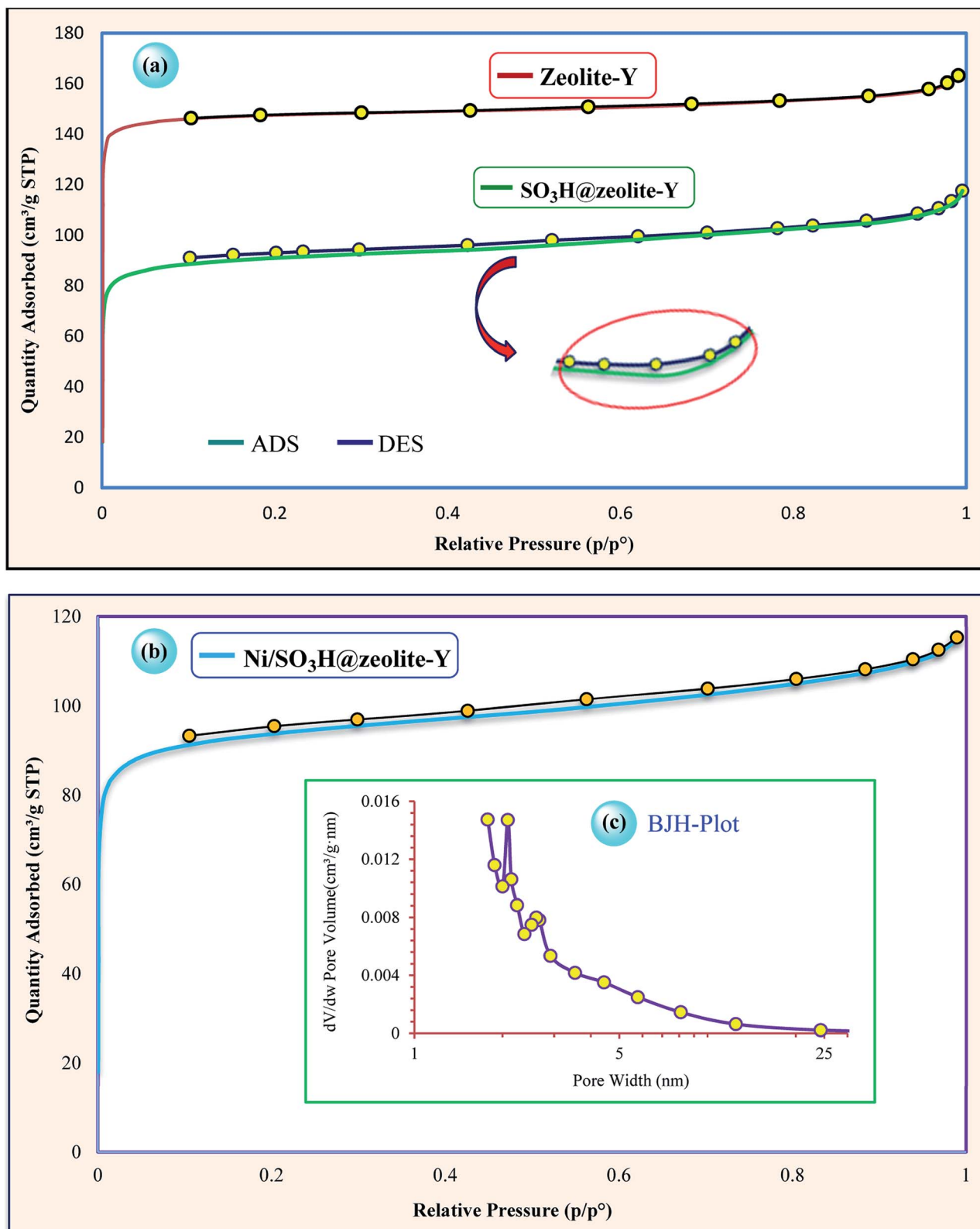


Fig. 5 N_2 adsorption/desorption isotherms of (a) zeolite-NaY and $SO_3H@zeolite-Y$, (b and c) N_2 ads./des. isotherm and BJH pore size distributions of $Ni/SO_3H@zeolite-Y$.

$SO_3H@zeolite-Y$ and $Ni/SO_3H@zeolite-Y$, it can be concluded that as a nanoporous $Ni/SO_3H@zeolite-Y$ is the best catalyst due to reduced reaction time and increased product

efficiency. Looking at Table 2 shows that the reaction yields increases in the aprotic-protic polar solvent mixture (water/acetone). This may be due to the type of mechanism



Table 1 Porosimetry values for zeolite-NaY and its modified structures

| Samples | S_{BET}^a ($\text{m}^2 \text{g}^{-1}$) | V_{BJH}^b ($\text{cm}^3 \text{g}^{-1}$) | D_{BJH}^c (nm) | D_{Aap}^d (nm) | P_{APS}^e (nm) |
|---|--|---|----------------------------|----------------------------|----------------------------|
| Zeolite-NaY | 441 | 0.032 | 6.73 | 2.21 | 13.6 |
| $\text{SO}_3\text{H}@zeolite\text{-}Y$ | 285 | 0.053 | 5.15 | 2.35 | 21.1 |
| Ni/ $\text{SO}_3\text{H}@zeolite\text{-}Y$ | 298 | 0.049 | 5.14 | 2.37 | 20.7 |

^a Specific surface area. ^b Pore volume. ^c Pore size (calculated from the adsorption branch). ^d Adsorption average pore diameter ($4V/A$ by BET). ^e Average particle size (estimated using the Temkin method).

proposed (Scheme 3) and the better performance of the multi-functional nanocatalyst in the water-acetone solvent mixture.

To demonstrate the versatility and uniqueness of this catalytic transformation, a variety of aromatic aldehydes were converted into corresponding *N*-benzimidazolyl(thiazolyl)-1,3-thiazolidin-4-ones in term of low reaction times and high yields at room temperature. As shown in Table 3, in all cases, aromatic aldehydes with substituents carrying either electron-donating (OH, OMe) or electron-withdrawing groups (Cl, Br, NO_2) reacted successfully and gave the expected products in excellent yields and short reaction times.

3.2.2. Reaction mechanism in the presence of catalyst. The suggested mechanism of formation of 1,3-thiazolidin-4-ones catalyzed by the Ni/ $\text{SO}_3\text{H}@zeolite\text{-}Y$ is shown in Scheme 3. At the beginning of this catalytic reaction, nano-Ni/ $\text{SO}_3\text{H}@zeolite\text{-}Y$ activates the carbonyl group of the aldehyde by the SO_3H functional group and Ni^{2+} on the surface of zeolite to produce intermediate 2'a-j.

Afterwards, 2-aminobenzimidazole (2-aminobenzothiazole) as a nucleophile attacks activated aldehyde to afford the species

5 that is followed by catalytic oxidation process and remove a H_2O molecule to produce the Schiff base **I**. In second catalytic activating stage, the nucleophilic attack of thioglycolic acid takes place to form the third intermediate **II**. Finally, after intermolecular nucleophilic attack and the loss of the another H_2O molecule, cyclization of the 1,3-thiazolidin-4-one products **4a-p** can be done.

3.2.3. Catalytic potential. To study the reusable ability of the catalyst, the Ni/ $\text{SO}_3\text{H}@zeolite\text{-}Y$ was recovered from the reaction mixture at the end of each run by simple filtration, and then washed with ethyl acetate and dried at 80°C . The recycled Ni/ $\text{SO}_3\text{H}@zeolite\text{-}Y$ was tested for more runs under optimized reaction conditions, and its activity showed that catalyst has a good reusability even after five runs (Table 4). Also, the Ni content in the nanocatalyst was 21% w/w (atomic absorption analysis) before the catalytic run, while after the fifth reaction cycle, was marginally decreased to 20.4% w/w (this reduction can be due to the error in experimental chemical analysis).

The basic structure of the reused catalyst was also confirmed with FT-IR spectra. Fig. 7 has indicated that there is no difference in the FT-IR the fresh and the recovered zeolitic catalysts, approximately. As a result, the heterogeneous nature of the nanocatalyst is confirmed in this reaction and no noticeable leaching of amount of Ni or $-\text{SO}_3\text{H}$ groups has occurred. Also, this minimal reduction in nanocatalyst activity may be due to the nature and textural properties of the nanocomposite, such as reducing the specific surface area or filling a number of cavities.

The catalytic activity of Ni/ $\text{SO}_3\text{H}@zeolite\text{-}Y$ was compared with previously reported various catalysts for the preparation of 1,3-thiazolidin-4-one derivatives. The results are listed in Table 5. The good catalytic performance of the Ni/ $\text{SO}_3\text{H}@zeolite\text{-}Y$ nanocatalyst in comparison with other previously reported procedures, could be due to the fact that the acidic and metal sites existed on the catalyst.

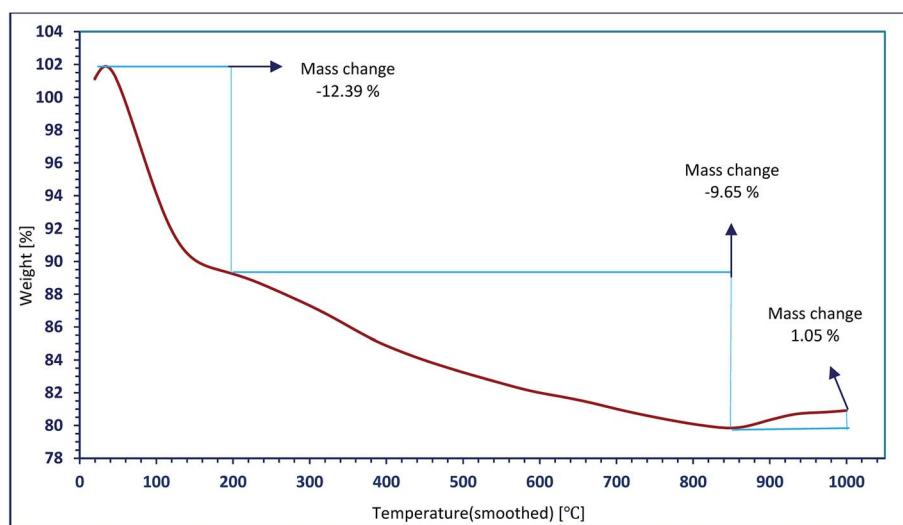
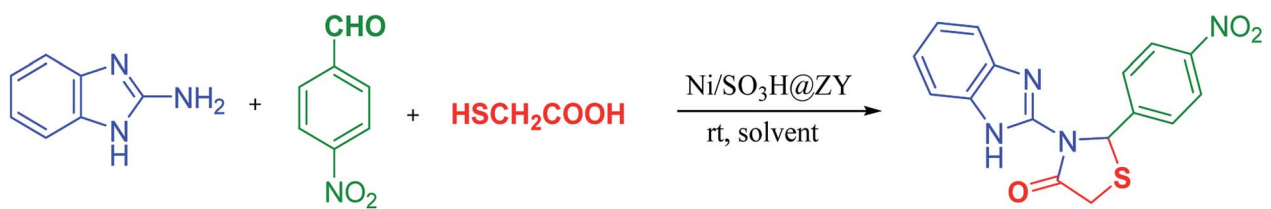
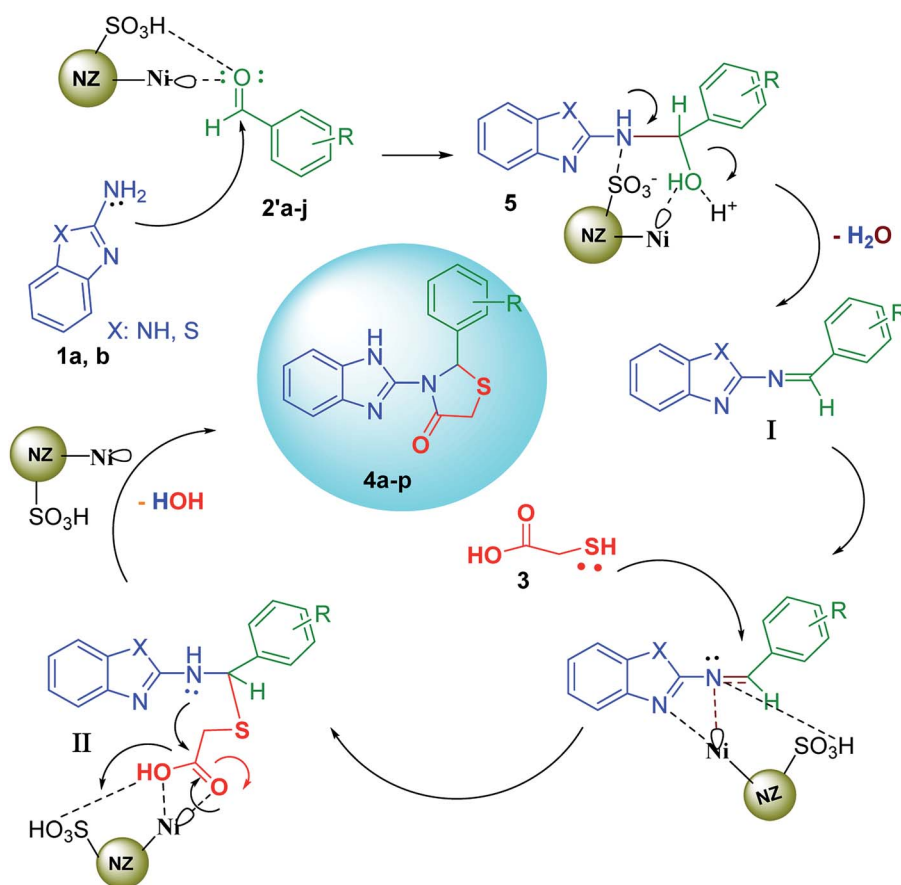
**Fig. 6** TGA curve of the Ni/ $\text{SO}_3\text{H}@zeolite\text{-}Y$.

Table 2 Optimizing the model reaction conditions at room temperature



| Entry | Catalyst loading (w/wt%) | Solvent | Time (min) | Yield ^a (%) |
|-------|--|----------------------------------|------------|------------------------|
| 1 | 5 | EtOH | 30 | 80 |
| 2 | 10 | EtOH | 25 | 90 |
| 3 | 10 | EtOH/H ₂ O (1 : 1) | 45 | 72 |
| 4 | 10 | Acetone | 30 | 87 |
| 5 | 10 | Acetone/H ₂ O (1 : 1) | 25 | 89 |
| 6 | 5 | Acetone/H ₂ O (1 : 1) | 15 | 97 |
| 7 | 3 | Acetone/H ₂ O (1 : 1) | 35 | 75 |
| 8 | 5 | H ₂ O | 60 | 30 |
| 9 | 5 | MeOH | 35 | 73 |
| 10 | 5 | CHCl ₃ | 60 | 43 |
| 11 | 5 | MeCN | 50 | 67 |
| 12 | 5 (NiCl ₂ ·2H ₂ O) | Acetone/H ₂ O (1 : 1) | 15 | 42 |
| 13 | 5 (SO ₃ H@ZY) | Acetone/H ₂ O (1 : 1) | 30 | 75 |
| 14 | 5 (zeolite-Y) | Acetone/H ₂ O (1 : 1) | 30 | Trace |
| 15 | — | Acetone/H ₂ O (1 : 1) | 240 | — |

^a Isolated yield.

Scheme 3 Proposed mechanism for the synthesis of compounds 4a–p.



Table 3 Synthesis of compounds **4a–p** in the presence of Ni/SO₃H@zeolite-Y at room temperature

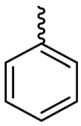
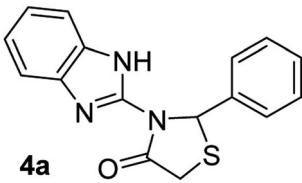
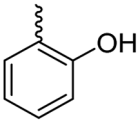
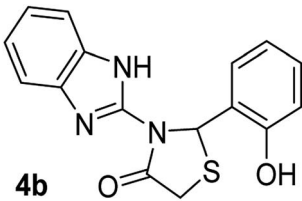
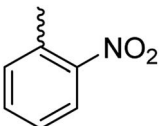
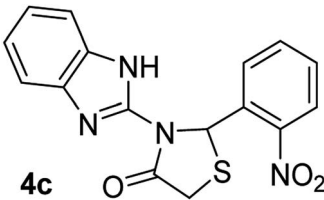
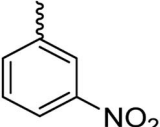
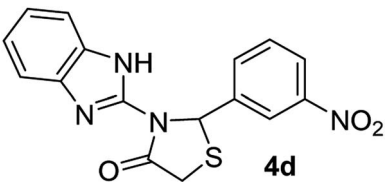
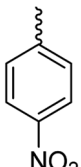
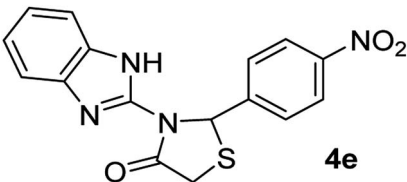
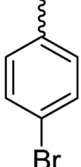
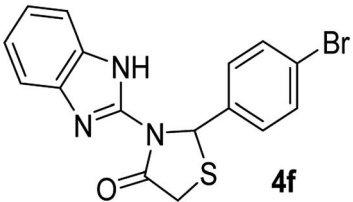
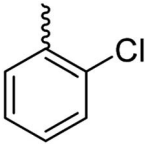
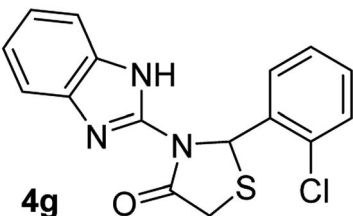
| Entry | Ar-CHO | Product | Time (min) | Mp (°C) | Yield ^a (%) |
|-------|---|--|------------|--------------------------------|------------------------|
| 1 |  |  4a | 20 | 209–210 (208–210) ^b | 85 |
| 2 |  |  4b | 22 | 245–246 (245–246) | 90 |
| 3 |  |  4c | 15 | 265–267 | 92 |
| 4 |  |  4d | 18 | 147–148 (146–148) | 90 |
| 5 |  |  4e | 15 | 208–210 (207–210) | 95 |
| 6 |  |  4f | 20 | 244–246 (244–246) | 94 |
| 7 |  |  4g | 20 | 221–223 | 89 |



Table 3 (Contd.)

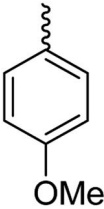
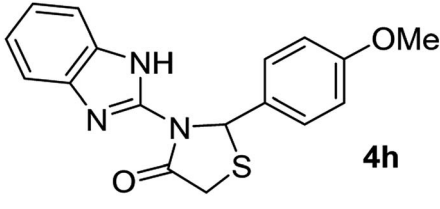
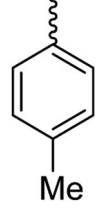
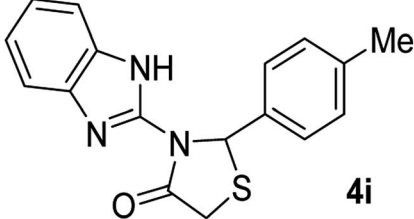
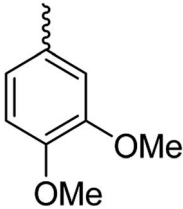
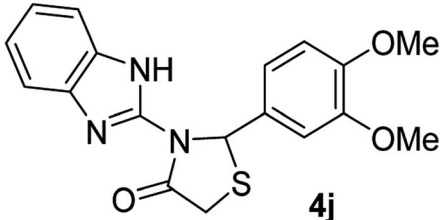
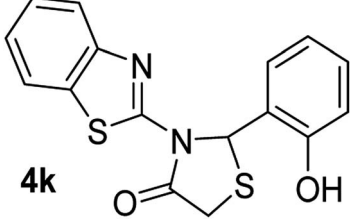
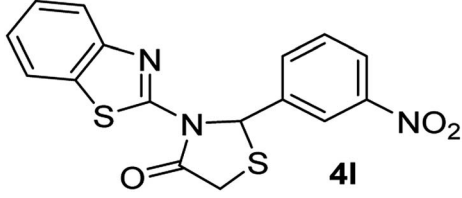
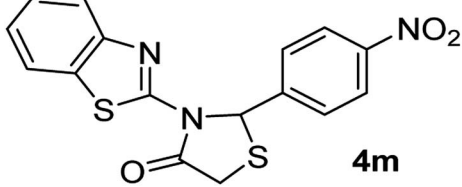
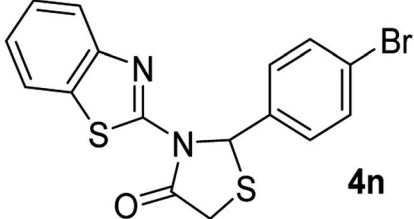
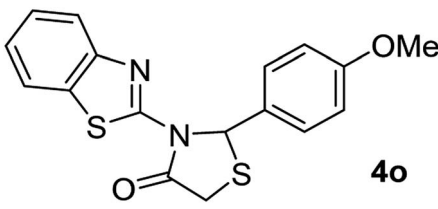
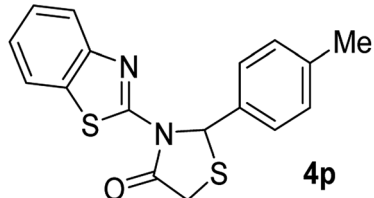
| Entry | Ar-CHO | Product | Time (min) | Mp (°C) | Yield ^a (%) |
|-------|---|---|------------|-------------------|------------------------|
| 8 |  |  4h | 25 | 216 (215–217) | 84 |
| 9 |  |  4i | 25 | 220 (221–223) | 87 |
| 10 |  |  4j | 22 | 167–169 (167–170) | 89 |
| 11 | 2b |  4k | 21 | 252–253 | 93 |
| 12 | 2d |  4l | 20 | 171–172 | 95 |
| 13 | 2e |  4m | 15 | 176 | 97 |
| 14 | 2f |  4n | 20 | 161–162 | 95 |



Table 3 (Contd.)

| Entry | Ar-CHO | Product | Time (min) | Mp (°C) | Yield ^a (%) |
|-------|--------|---|------------|---------|------------------------|
| 15 | 2h |  | 25 | 177–178 | 90 |
| 16 | 2i |  | 25 | 194–195 | 88 |

^a Isolated yields. ^b Melting points in parentheses are reported in the literature.³⁷

Table 4 Catalyst recovery study in the model reaction under optimized conditions

| Entry | Time (min) | Yield ^a (%) |
|-------|------------|------------------------|
| 1 | 15 | 97 |
| 2 | 15 | 97 |
| 3 | 15 | 93 |
| 4 | 15 | 92 |
| 5 | 15 | 89 |

^a Isolated yields.

Table 5 Comparison of the activity of various catalysts for the synthesis of 1,3-thiazolidin-4-ones

| Entry | Catalyst | Condition | Time (min) | Yield (%) |
|-------|--|------------------------------|------------|-------------------|
| 1 | DCC | THF, RT | 60 | (59–95) (ref. 36) |
| 2 | Ni@zeolite | EtOH, RT | 25–35 | (80–95) (ref. 5) |
| 3 | Pd NPs | Solvent-free, 100 °C | 60 | (71–90) (ref. 28) |
| 4 | Alum | MW, 100 °C | 4–5 | (86–98) (ref. 33) |
| 5 | Silica gel | THF, RT | 240–420 | (77–96) (ref. 29) |
| 6 | DIPEA | Toluene, reflux | 180–240 | (65–85) (ref. 31) |
| 7 | CoFe ₂ O ₄ @SiO ₂ /Pr-NH ₂ | PhCH ₃ , reflux | 120–480 | (75–85) (ref. 35) |
| 8 | Catalyst-free | H ₂ O, RT | 240–420 | (79–96) (ref. 32) |
| 9 | HClO ₄ -SiO ₂ | PhCH ₃ , 100 °C | 180–360 | (70–88) (ref. 30) |
| 10 | La(NO ₃) ₃ | EtOH, RT | 24 | (77–90) (ref. 37) |
| 11 | MCM-41@Si-L, CuSO ₄ | PhCH ₃ , 110 °C | 720 | (77–99) (ref. 41) |
| 12 | Fe ₃ O ₄ @SiO ₂ /APTOSS | Solvent-free, 60 °C | 30 | (90–94) (ref. 42) |
| 13 | Ni/SO ₃ H@zeolite-Y | H ₂ O–acetone, RT | 15–25 | 85–97 (This work) |

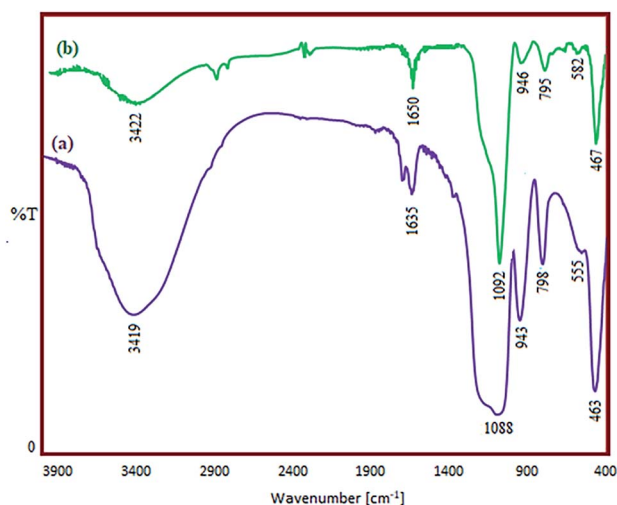


Fig. 7 FT-IR spectra of (a) the fresh catalyst and (b) the five-times reused catalyst.

4. Conclusion

In conclusion, the SO₃H@zeolite-Y supported Ni has been synthesized successfully and found to be a highly efficient and multi-functionalized nanocatalyst for the three-component synthesis of 3-benzimidazolyl or benzthiazolyl-1,3-thiazolidin-4-ones under green conditions. This procedure offers several advantages, including improving the reaction



performance, operational simplicity without high temperature, exceptionally fast, high yields, low cost, non-toxic nature of the nanocatalyst, and reusability of the catalyst.

Conflicts of interest

There are no conflicts to declare.

Acknowledgements

We are grateful to the research commute of Payame Noor University for providing financial and technical supports for this work.

References

- 1 J. Liang, Z. Liang, R. Zou and Y. Zhao, *Adv. Mater.*, 2017, **29**, 1701139.
- 2 G. Perot and M. Guisnet, *J. Mol. Catal.*, 1990, **61**, 173–196.
- 3 (a) C. G. S. Lima, N. M. Moreira, M. W. Paixão and A. G. Corrêa, *Curr. Opin. Green Sustain. Chem.*, 2019, **15**, 7–12; (b) M. M. Heravi, B. Heidari, V. Zadsirjan and L. Mohammadi, *RSC Adv.*, 2020, **10**, 24893–24940.
- 4 M. Zendehele, M. A. Bodaghifard, H. Behyar and Z. Mortezaei, *Microporous Mesoporous Mater.*, 2018, **266**, 83–89.
- 5 M. Kalhor, S. Banibairami and S. A. Mirshokraie, *Green Chem. Lett. Rev.*, 2018, **11**, 334–344.
- 6 M. Kalhor and N. Khodaparast, *Res. Chem. Intermed.*, 2015, **41**, 3235–3242.
- 7 N. Miskolczi, T. Juzsakova and J. Sója, *J. Energy Inst.*, 2019, **92**, 118–127.
- 8 X. Fu, X. Sheng, Y. Zhou, Z. Fu, S. Zhao, X. Bu and C. Zhang, *RSC Adv.*, 2016, **6**, 50630–50639.
- 9 M. M. Khakzad Siuki, M. Bakavoli and H. Eshghi, *Appl. Organomet. Chem.*, 2019, e4774.
- 10 A. Tadjarodi, M. Dehghani and M. Imani, *Appl. Organomet. Chem.*, 2018, e4594.
- 11 R. Estevez, I. Iglesias, D. Luna and F. M. Bautista, *Molecules*, 2017, **22**, 2206–2218.
- 12 N. Krathumkhetb, K. Vongjitpimolb, T. Chuesuthamb, S. Changkhamchoma, K. Phasuksoma, A. Sirivata and K. Wattanakulb, *Solid State Ionics*, 2018, **319**, 278–284.
- 13 H. Nur, G. L. Kee, H. Hamdan, T. M. I. Mahlia, J. Efendi and H. S. C. Metselaar, *Int. J. Hydrogen Energy*, 2012, **37**, 12513–12521.
- 14 R. Kumar, V. Strezov, E. Lovell, T. Kan, H. Weldekidan, J. He, S. Jahan, B. Dastjerdi and J. Scott, *J. Anal. Appl. Pyrolysis*, 2019, **140**, 148–160.
- 15 A. Quindimil, U. De-La-Torre, B. Pereda-Ayo, J. A. González-Marcos and J. R. González-Velasco, *Appl. Catal., B*, 2018, **238**, 393–403.
- 16 S. U. Lee, Y. J. Lee, J. R. Kim and S. Y. Jeong, *J. Ind. Eng. Chem.*, 2018, **66**, 279–287.
- 17 J. Cheng, Z. Zhang, X. Zhang, J. Liu, J. Zhou and K. Cen, *Fuel*, 2019, **245**, 384–391.
- 18 M. Kalhor and Z. Zarnegar, *RSC Adv.*, 2019, **9**, 19333–19346.
- 19 (a) D. Jagadeesan, *Appl. Catal., A*, 2016, **511**, 59–77; (b) H. Zhang, Y. Zhang, Y. Zhou, C. Zhang, Q. Wang, Y. Xua and M. Zhang, *RSC Adv.*, 2016, **6**, 18685–18694.
- 20 (a) W. Cunico, C. R. B. Gomes and W. T. Vellasco Junior, *Mini-Rev. Org. Chem.*, 2008, **5**, 336–344; (b) A. K. Jain, A. Vaidya, V. Ravichandran and S. K. Kashaw, *Bioorg. Med. Chem.*, 2012, **20**, 3378–3395.
- 21 (a) B. C. C. Cantello, M. A. Cawthorne, D. Haigh, R. M. Hindley, S. A. Smith and P. L. Thurlby, *Bioorg. Med. Chem. Lett.*, 1994, **4**, 1181–1184; (b) S. K. Manjal, R. Kaur, R. Bhatia, K. Kumar, V. Singh, R. Shankar, R. Kaur and R. K. Rawal, *Bioorg. Chem.*, 2017, **75**, 406–423; (c) A. Mobinikhaledi, N. Foroughifar, M. Kalhor and M. Mirabolfathy, *J. Heterocycl. Chem.*, 2010, **47**, 77–80.
- 22 (a) V. K. Kapoor, S. Dubey and N. Mahindroo, *Indian J. Chem.*, 2000, **39B**, 27–30; (b) R. Dahiya, *Sci. Pharm.*, 2008, **76**, 217–239.
- 23 (a) H. J. Breslin, C. A. Cai, T. Miskowski, S. V. Coutinho, S. P. Zhang and H. Pamela, *Bioorg. Med. Chem. Lett.*, 2006, **16**, 2505–2508; (b) M. R. Yadav, D. S. Puntambekar, K. P. Sarathy, S. Vengurlekar and R. Giridhar, *Indian J. Chem.*, 2006, **45**, 475–782; (c) S. Khabnadi-deh, Z. Rezaei, A. Khalafi-Nezhad, R. Bahrinajafi and R. F. Mohamadi, *Bioorg. Med. Chem. Lett.*, 2003, **13**, 2863–2865.
- 24 A. Deep, B. Narasimhan, V. Mani, K. Ramasamy, R. K. Mishra and S. Lim, *RSC Adv.*, 2016, **6**, 109485–109494.
- 25 N. Foroughifar and S. Ebrahimi, *Chin. Chem. Lett.*, 2013, **24**, 389–391.
- 26 P. Cheng, W. Guo, P. Chen, Y. Liu, X. Du and C. Li, *Chem. Commun.*, 2016, **52**, 3418–3421.
- 27 H. X. Pang, Y. H. Hui, K. Fan, X. J. Xing, Y. Wu, J. H. Yang and W. Z. F. Xie, *Chin. Chem. Lett.*, 2016, **27**, 335–339.
- 28 R. R. Harale, P. V. Shitre, B. R. Sathe and M. S. Shingare, *Res. Chem. Intermed.*, 2016, **42**, 6695–6703.
- 29 M. P. Thakare, P. Kumar, N. Kumar and S. K. Pandey, *Tetrahedron Lett.*, 2014, **55**, 2463–2466.
- 30 D. Kumar, M. Sonawane, B. Pujala, V. K. Jain, S. Bhagat and A. K. Chakraborti, *Green Chem.*, 2013, **15**, 2872–2884.
- 31 A. V. Chate, A. G. Tathe, P. J. Nagtilak, S. M. Sangle and C. H. Gill, *Chin. J. Catal.*, 2016, **37**, 1997–2002.
- 32 M. P. Thakare, R. Shaikh and D. Tayade, *RSC Adv.*, 2016, **6**, 28619–28623.
- 33 S. A. Jadhav, M. G. Shioorkar, O. S. Chavan, S. Jadhav, M. Shioorkar, O. S. Chavan, D. B. Shinde and R. K. Pardeshi, *Heterocycl. Lett.*, 2015, **5**, 375–382.
- 34 S. M. Sadeghzadeh and M. Malekzadeh, *J. Mol. Liq.*, 2015, **202**, 46–51.
- 35 J. Safaei-Ghomi, M. Navvab and H. Shahbazi-Alavi, *J. Sulfur Chem.*, 2016, **37**, 601–612.
- 36 T. Srivastava, W. Haq and S. B. Katti, *Tetrahedron*, 2001, **58**, 7619–7624.
- 37 M. Kalhor, S. Banibairami and S. A. Mirshokraie, *Res. Chem. Intermed.*, 2017, **43**, 5985–5994.
- 38 S. Ebrahimi, *J. Sulfur Chem.*, 2016, **37**, 587–592.



- 39 F. Rouquerol, J. Rouquerol and K. S. W. Sing, *Adsorption by Powder and Porous Solids*, Academic press, San Diego, 1999, pp. 1–25.
- 40 K. Sarkar, K. Dhara, M. Nandi, P. Roy, A. Bhaumik and P. Banerjee, *Adv. Funct. Mater.*, 2009, **19**, 223–234.
- 41 H. X. Pang, Y. H. Hui, K. Fan, X. J. Xing, Y. Wu, J. H. Yang, W. Shi and Z. F. Xie, *Chin. Chem. Lett.*, 2016, **27**, 335–339.
- 42 J. Safaei-Ghomi, S. H. Nazemzadeh and H. Shahbazi-Alavi, *Appl. Organomet. Chem.*, 2016, e3520.

